Scattering-based decomposition of sensitivity kernels for full-waveform inversion

Daniel Leal Macedo* (Universidade Estadual de Campinas) and Ivan Vasconcelos (Schlumberger Cambridge Research)

Abstract

With the increasing demand in complexity for subsurface models in environments such as subsalt, sub-basalt and pre-salt, full-waveform inversion (FWI) is quickly becoming one of the model-building methods of choice. While in principle capable of handling all of the nonlinearity in the data, in practice nonlinear gradient-based FWI is limited due to its notorious sensitivity to the choice of starting models. To help addressing model convergence issues in FWI, in this paper we analyze the role of nonlinearity in the so-called sensitivity kernels, which are the centerpiece of gradient-based FWI algorithms. Using a scattering-based approach and assuming acoustic-only data, we start by reparameterizing the subsurface model in terms of smooth and singular components for both compressibility and density. This leads to a decomposition of the data into a reference field that is sensitive only to the smooth model, and a scattered field sensitive to both smooth and sharp model components. Focussing on the model backprojections from the scattered data only, we provide expressions for the Fréchet-derivative sensitivity kernels of all four model parameters. Our results provide for the decomposition of current FWI kernels into no less than nine different sub-kernels which have explicitly different levels of nonlinearity with respect to both data and model parameters. This capability to discern levels of nonlinearity within FWI kernels is key to understanding model convergence in gradient-based, iterative FWI. We illustrate this by analyzing some of the sub-kernel terms in detail. The scattering-based FWI kernel decomposition we provide could have broad potential applications, such devising multiscale FWI algorithms, and improving velocity model building in the image domain using extended image gathers.

Introduction

For many years, the most common imaging techniques were based on ray theory, such as, Kirchhoff migration. But lately, as the industry have been facing geologically more complex areas where these techniques were not successful, new methods based on wave-equation migration came into play – in the begining, one-way wave-equation based, and more recently, two-way wave-equation. All this became possible due to new aquisition techniques which give better illumination of the subsurface, and more powerful computational capacities.

But those new methods require more and more refined Earth models. on the other, hand, even if migration has advanced quickily with computer power, constructing these models is still ray-based. Recently, one tool, based on the two-way wave-equation, have been studied and developed for Earth modeling: The *full waveform inversion (FWI)* (Vigh et al., 2009).

The basic idea behind the FWI is the minimization of a objective function that ”mesures” the difference between observed seismic data and synthetic data from a earth model. In the last decades, many studies on FWI were made. On Virieux and Operto (2009) and Vigh et al. (2009) one can find the state-of-art on the subject.

A series of paper publish on the eighties (Lailly, 1983; Tarantola, 1984, 1986) brought to light the gradient-based FWI in the applied geophysics field. In a few words, this methods says that a model can be updated iteratively with the help of the *sensitivity kernels (SK)*. The SK's are operators that give the change in the wavefield due to changes in the model parameters. With the adjoint of the SK, one can evaluate the change in the earth model due to wavefield residuals.

While in principle capable of handling all of the nonlinearity in the data, in practice nonlinear gradient-based FWI is limited due to its notorious sensitivity to the choice of starting models. To help addressing model convergence issues in FWI, in this paper we analyze the role of nonlinearity in the sensitivity kernels.

To do so, we use a scattering-based approach (Vasconcelos, 2008). Assuming a acoustic medium, we reparameterize the subsurface model in terms of smooth and singular components for both compressibility and density. This leads to a decomposition of the data into a reference field that is sensitive only to the smooth model, and a scattered field sensitive to both smooth and sharp model components.

Focussing on the model backprojections from the scattered data only, we provide expressions for the Fréchet-derivative sensitivity kernels of all four model parameters.

The scattering-based FWI kernel decomposition we provide could have broad potential applications, such devising multiscale FWI algorithms, and improving velocity model building in the image domain using extended image (EI) gathers (Rickett and Sava, 2002; Sava and Fomel, 2003; Symes, 2008; Sava and Vasconcelos, 2009, 2010). As shown by Vasconcelos et al. (2009, 2010), there's a connection between the extended image conditions and the interferometry formalism: the EI's behave like locally scattered wavefields in the image domain.

Sensitivity kernels

The acoustic wave equation states a non-linear relation between the wavefield and the model parameters, which can be written as

$$G = f(\boldsymbol{m}). \tag{1}$$

where G is the acoustic wavefield and $\boldsymbol{m}$ are the model parameters.

The sensitivity kernel $\boldsymbol{\Phi}_f$ apears when a disturbance $\boldsymbol{\delta m}$ is introduced in the model parameters, so that

$$G + \delta G^{true} = f(\boldsymbol{m} + \boldsymbol{\delta m}) = f(\boldsymbol{m}) + \boldsymbol{\Phi}_f \boldsymbol{\delta m} + O(\boldsymbol{\delta m}^2) \tag{2}$$

where δG^{true} is the change in the wavefield. If only first-order terms on the model changes are taken into account, we get the linearized change in the wavefield, δG,

$$\delta G = \boldsymbol{\Phi}_f \boldsymbol{\delta m} \tag{3}$$

The expression for $\boldsymbol{\Phi}_f$ is obtained from the *secondary sources* (Tarantola, 1984), which can be seen as pseudo-sources that give rises to changes in the wavefield due to changes in the model parametrers. Given the acoustic wave-equation

$$\mathcal{L}(\boldsymbol{x}) G(\boldsymbol{x}, t; \boldsymbol{x}_s) = \delta(\boldsymbol{x} - \boldsymbol{x}_s)\delta(t - t_0) \tag{4}$$

with

$$\mathcal{L}(\boldsymbol{x}) = \left\{ \frac{1}{K(\boldsymbol{x})} \frac{\partial^2}{\partial t^2} - \nabla_x \cdot \left(\frac{1}{\rho(\boldsymbol{x})} \nabla_x \right) \right\}; \tag{5}$$

where K is the bulk modulus, ρ is the density, and G is the Green's function respectively[1]. Introducing a model pertubation – δK and $\delta\rho$ – in the operator $\mathcal{L}$, and taking its first-order contribution gives us

$$\mathcal{L}(\boldsymbol{x}) \delta G(\boldsymbol{x}, t; \boldsymbol{x}_s) = -\delta\mathcal{L}(\boldsymbol{x}) G(\boldsymbol{x}, t; \boldsymbol{x}_s). \tag{6}$$

where the *full secondary potencial*, $\delta\mathcal{L}$, is defined as

$$\delta\mathcal{L}(\boldsymbol{x}) = -\left\{ \frac{\delta K(\boldsymbol{x})}{K^2(\boldsymbol{x})} \frac{\partial^2}{\partial t^2} - \nabla_x \cdot \left(\frac{\delta\rho(\boldsymbol{x})}{\rho^2(\boldsymbol{x})} \nabla_x \right) \right\}. \tag{7}$$

The right-hand side of (6) is the sencondary source, which can be forward propagated to give δG[2]:

$$\delta G(\boldsymbol{x}, t; \boldsymbol{x}_s) = -\int_{\mathbb{V}} d^3\boldsymbol{x}'\, G(\boldsymbol{x}, t; \boldsymbol{x}') * \delta\mathcal{L}(\boldsymbol{x}') G(\boldsymbol{x}', t; \boldsymbol{x}_s). \tag{8}$$

In the frequency domain[3], the expression above can be written in matrix notation as

$$\widehat{\delta G}(\boldsymbol{x}_g; \boldsymbol{x}_s) = \boldsymbol{\Phi}_f \boldsymbol{\delta m} = \begin{bmatrix} \boldsymbol{U}_f & \boldsymbol{V}_f \end{bmatrix} \begin{bmatrix} \boldsymbol{\delta K} \\ \boldsymbol{\delta\rho} \end{bmatrix}. \tag{9}$$

From the expression above, the weighted changes in the bulk modulus, $\boldsymbol{\delta K^k}$, and density, $\boldsymbol{\delta\rho^k}$, are obtained from the wavefield residual $\widehat{\delta G}$ by[4]

$$\begin{bmatrix} \boldsymbol{\delta K^k} \\ \boldsymbol{\delta\rho^k} \end{bmatrix} = \boldsymbol{\delta m^k} = \boldsymbol{\Phi}_f^\dagger \widehat{\delta G} = \begin{bmatrix} \boldsymbol{U}_f^\dagger \\ \boldsymbol{V}_f^\dagger \end{bmatrix} \widehat{\delta G}. \tag{10}$$

[1] For simplicity sake, from time to time the variable dependencies will be droped out.

[2] The symbol $*$ denotes time-convolution

[3] The Fourier transform of a wavefield p is $\hat{p}(\boldsymbol{x}, \omega; \boldsymbol{x}_s) = \int_{-\infty}^{\infty} p(\boldsymbol{x}, t; \boldsymbol{x}_s) e^{-i\omega t}\, dt$.

[4] The symbol † stands for adjoint matrix.

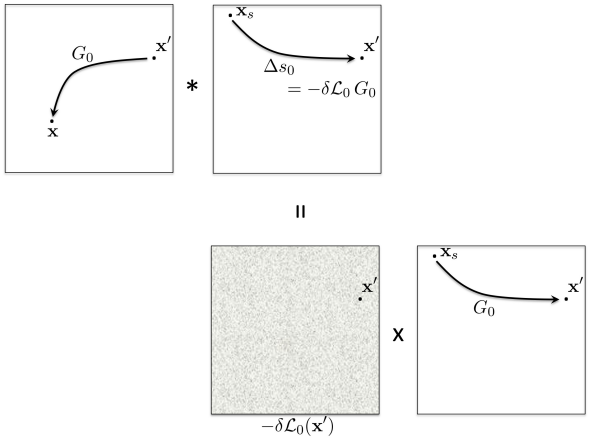

Figure 1: δG_0 evaluated at $\boldsymbol{x}$ for a source at $\boldsymbol{x}_s$. For each $\boldsymbol{x}'$ may there be a secondary source $-\delta\mathcal{L}_0 G_0$ which contributes to δG_0 (botton). Then, this source is propagated to $\boldsymbol{x}$ (top). Contributions from all $\boldsymbol{x}'$ are then integrated.

Wavefield separation and sensitivity kernels

The same ideia summarized above is applied on the system of wave-equations for the reference and scattered wavefields (Vasconcelos, 2008) shown below

$$\mathcal{L}_0 G_0 = \delta(\boldsymbol{x} - \boldsymbol{x}_s)\,\delta(t - t_0), \tag{11}$$

$$\mathcal{L} G_S = -\mathcal{V} G_0, \tag{12}$$

with

$$\mathcal{L}_0 = \left\{ \frac{1}{K_0} \frac{\partial^2}{\partial t^2} - \nabla \cdot \left(\frac{1}{\rho_0} \nabla \right) \right\}; \tag{13}$$

$$\mathcal{L} = \left\{ \frac{1}{K_0 + \Delta K} \frac{\partial^2}{\partial t^2} - \nabla \cdot \left(\frac{1}{\rho_0 + \Delta\rho} \nabla \right) \right\}; \tag{14}$$

$$\mathcal{V} = \mathcal{L} - \mathcal{L}_0, \tag{15}$$

where K_0 and ρ_0 stands for the smooth (reference) part of the model, ΔK and $\Delta\rho$ represent the singular one, i.e., $K = K_0 + \Delta K$ and $\rho = \rho_0 + \Delta\rho$; and G_0 and G_S are the reference and scattered wavefields, respectively, so that $G = G_0 + G_S$.

The secondary sources for (11) due to model pertubations δK_0 and $\delta\rho_0$ introduced in $\mathcal{L}_0$ is analogous to the one for (4), so that

$$\mathcal{L}_0(\boldsymbol{x})\, \delta G_0(\boldsymbol{x}, t; \boldsymbol{x}_s) = -\delta\mathcal{L}_0(\boldsymbol{x}) G_0(\boldsymbol{x}, t; \boldsymbol{x}_s), \tag{16}$$

where $\delta\mathcal{L}_0$ is the same of (7) but the replacement of K and ρ for K_0 and ρ_0, respectively. This potencial is called *reference secondary potencial*, which allows us to evaluate the change in the reference wavefield, δG_0,

$$\delta G_0(\boldsymbol{x}, t; \boldsymbol{x}_s) = -\int_{\mathbb{V}} d^3\boldsymbol{x}'\, G_0(\boldsymbol{x}, t; \boldsymbol{x}') * \delta\mathcal{L}_0(\boldsymbol{x}') G_0(\boldsymbol{x}', t; \boldsymbol{x}_s). \tag{17}$$

A cartoon representing the operation described above can be seen in Figure 1.

Introducing model pertubations δK_0, $\delta\rho_0$, $\delta\Delta K$ and $\delta\Delta\rho$ in operators $\mathcal{L}$ and $\mathcal{L}_0$ of (12), we arrive in the expression of

the secondary sources, Δs, for the change in the scattered wavefield, δG_S,

$$\begin{aligned}\mathcal{L}(\boldsymbol{x})\,\delta G_S(\boldsymbol{x},t;\boldsymbol{x}_s) &= \Delta s(\boldsymbol{x},t;\boldsymbol{x}_s)\\ &= -\mathcal{V}(\boldsymbol{x})\,\delta G_0(\boldsymbol{x},t;\boldsymbol{x}_s)-\delta\mathcal{L}(\boldsymbol{x})\,G(\boldsymbol{x},t;\boldsymbol{x}_s)\\ &\quad +\delta\mathcal{L}_0(\boldsymbol{x})\,G_0(\boldsymbol{x},t;\boldsymbol{x}_s),\end{aligned} \tag{18}$$

with (7) rewritten as

$$\delta\mathcal{L}=-\left\{\left(\frac{\delta K_0+\delta\Delta K}{(K_0+\Delta K)^2}\right)\frac{\partial^2}{\partial t^2}-\nabla\cdot\left[\left(\frac{\delta\rho_0+\delta\Delta\rho}{(\rho_0+\Delta\rho)^2}\right)\nabla\right]\right\}, \tag{19}$$

which allows us to evaluate the change in the scattered wavefield, δG_s, by

$$\delta G_S(\boldsymbol{x},t;\boldsymbol{x}_s)=\int_{\mathbb{V}}d^3\boldsymbol{x}'\,G(\boldsymbol{x}',t;\boldsymbol{x})*\Delta s(\boldsymbol{x}',t;\boldsymbol{x}_s). \tag{20}$$

Expression (20) can be decomposed in 8 terms:

$$\begin{aligned}\delta G_S(\boldsymbol{x},t;\boldsymbol{x}_s) &= -\Big\{\int_{\mathbb{V}}d^3\boldsymbol{x}'\,G_0(\boldsymbol{x}',t;\boldsymbol{x})*\mathcal{V}(\boldsymbol{x}')\,\delta G_0(\boldsymbol{x}',t;\boldsymbol{x}_s)+\\ &\int_{\mathbb{V}}d^3\boldsymbol{x}'\,G_S(\boldsymbol{x}',t;\boldsymbol{x})*\mathcal{V}(\boldsymbol{x}')\,\delta G_0(\boldsymbol{x}',t;\boldsymbol{x}_s)+\\ &\int_{\mathbb{V}}d^3\boldsymbol{x}'\,G_0(\boldsymbol{x}',t;\boldsymbol{x})*\delta\mathcal{L}(\boldsymbol{x}')\,G_0(\boldsymbol{x}',t;\boldsymbol{x}_s)+\\ &\int_{\mathbb{V}}d^3\boldsymbol{x}'\,G_S(\boldsymbol{x}',t;\boldsymbol{x})*\delta\mathcal{L}(\boldsymbol{x}')\,G_0(\boldsymbol{x}',t;\boldsymbol{x}_s)+\\ &\int_{\mathbb{V}}d^3\boldsymbol{x}'\,G_0(\boldsymbol{x}',t;\boldsymbol{x})*\delta\mathcal{L}(\boldsymbol{x}')\,G_S(\boldsymbol{x}',t;\boldsymbol{x}_s)+\\ &\int_{\mathbb{V}}d^3\boldsymbol{x}'\,G_S(\boldsymbol{x}',t;\boldsymbol{x})*\delta\mathcal{L}(\boldsymbol{x}')\,G_S(\boldsymbol{x}',t;\boldsymbol{x}_s)\Big\}+\\ &\int_{\mathbb{V}}d^3\boldsymbol{x}'\,G_S(\boldsymbol{x}',t;\boldsymbol{x})*\delta\mathcal{L}_0(\boldsymbol{x}')\,G_0(\boldsymbol{x}',t;\boldsymbol{x}_s)+\\ &\int_{\mathbb{V}}d^3\boldsymbol{x}'\,G_0(\boldsymbol{x}',t;\boldsymbol{x})*\delta\mathcal{L}_0(\boldsymbol{x}')\,G_0(\boldsymbol{x}',t;\boldsymbol{x}_s).\end{aligned} \tag{21}$$

Each of this terms gives contributions of different order to δG_S. The Figures from 2 to 9 show cartoons representing the contributions of each term.

Model reparametrization an adjoint SK's

In the frequency domain, (17) and (20) can be written in matrix notation as

$$\widehat{\delta G}_0(\boldsymbol{x}_g;\boldsymbol{x}_s)=\begin{bmatrix}\boldsymbol{U_0} & \boldsymbol{V_0} & \boldsymbol{0} & \boldsymbol{0}\end{bmatrix}\begin{bmatrix}\boldsymbol{\delta K_0}\\ \boldsymbol{\delta\rho_0}\\ \boldsymbol{\delta\Delta K^k}\\ \boldsymbol{\delta\Delta\rho}\end{bmatrix}, \tag{22}$$

e

$$\widehat{\delta G}_S(\boldsymbol{x}_g;\boldsymbol{x}_s)=\begin{bmatrix}\boldsymbol{U} & \boldsymbol{V} & \boldsymbol{U_\Delta} & \boldsymbol{V_\Delta}\end{bmatrix}\begin{bmatrix}\boldsymbol{\delta K_0}\\ \boldsymbol{\delta\rho_0}\\ \boldsymbol{\delta\Delta K^k}\\ \boldsymbol{\delta\Delta\rho}\end{bmatrix}, \tag{23}$$

due to a reparametrization of the model.

From (21), we can write

$$\begin{aligned}\boldsymbol{\Phi} &= \begin{bmatrix}\boldsymbol{U} & \boldsymbol{V} & \boldsymbol{U_\Delta} & \boldsymbol{V_\Delta}\end{bmatrix}=\\ \sum_{i=1}^{n=8}\boldsymbol{\Phi}_i &= \sum_{i=1}^{n=8}\begin{bmatrix}\boldsymbol{U}_i & \boldsymbol{V}_i & \boldsymbol{U}_{\boldsymbol{\Delta},i} & \boldsymbol{V}_{\boldsymbol{\Delta},i}\end{bmatrix}.\end{aligned} \tag{24}$$

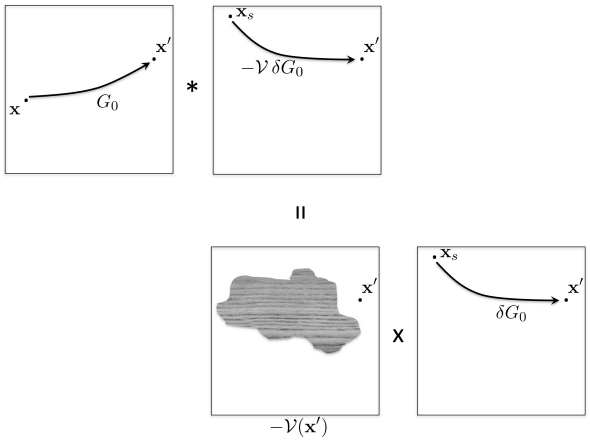

Figure 2: Term 1, Change in G_S due to single-scattering of the change in the reference wavefield by the scattering potential (singular part of the model).

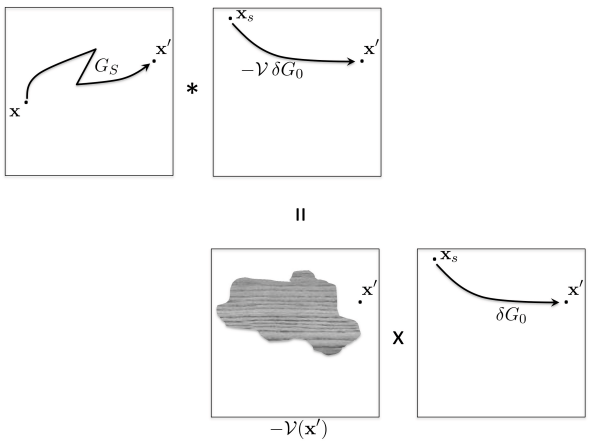

Figure 3: Term 2, Change in G_S due to multi-scattering of the change in the reference wavefield by the scattering potential (singular part of the model).

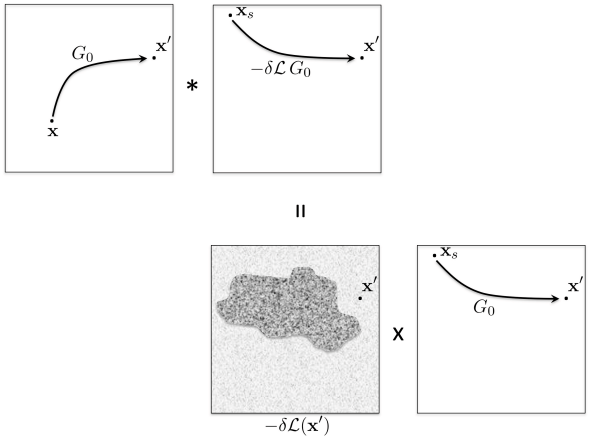

Figure 4: Term 3, Change in G_S due to single-scattering of the reference field by the full secondary potencial.

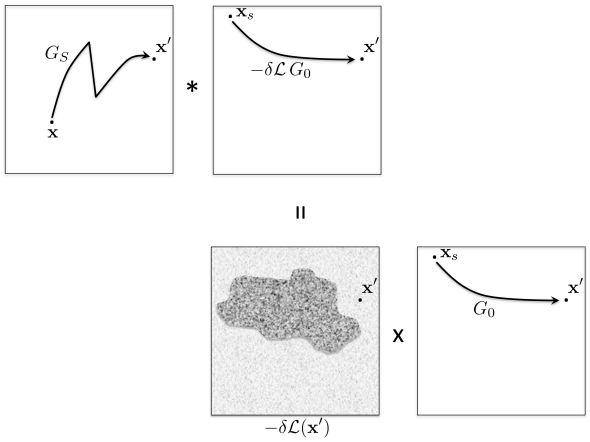

Figure 5: Term 4, Change in G_S due to multi-scattering of the reference field by the full secondary potencial.

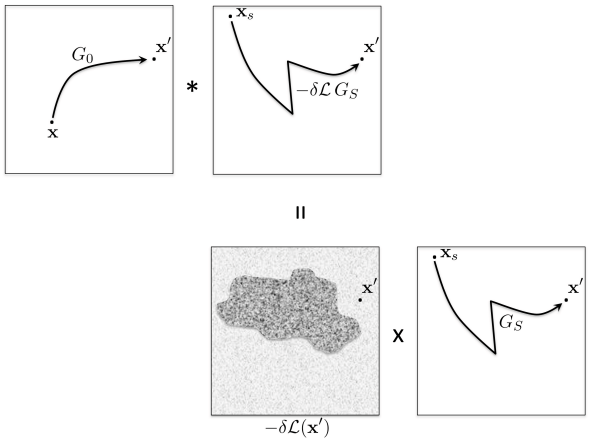

Figure 6: Term 5, Change in G_S due to single-scattering of the scattered field by the full secondary potencial.

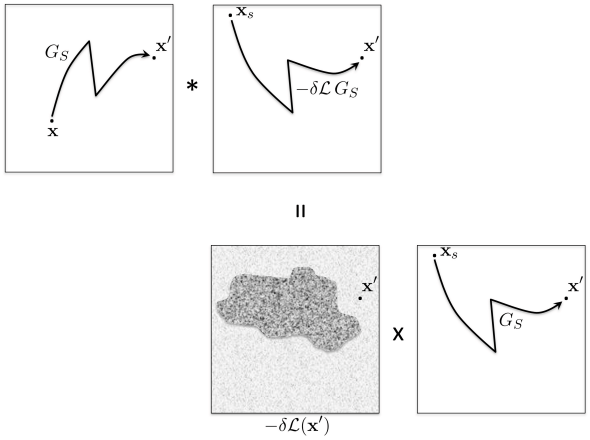

Figure 7: Term 6, Change in G_S due to multi-scattering of the scattered field by the full secondary potencial.

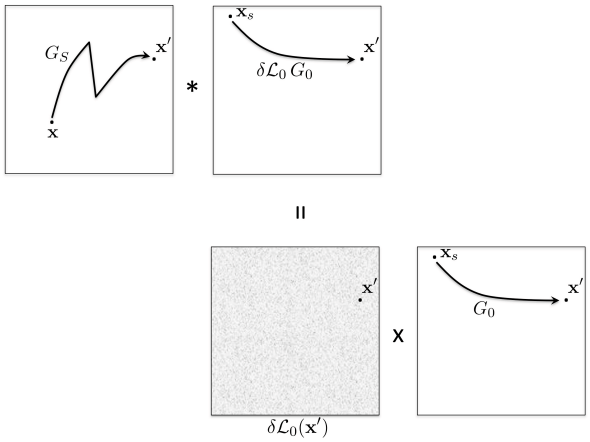

Figure 8: Term 7, Change in G_S due to multi-scattering of the reference field by the reference secondary potencial.

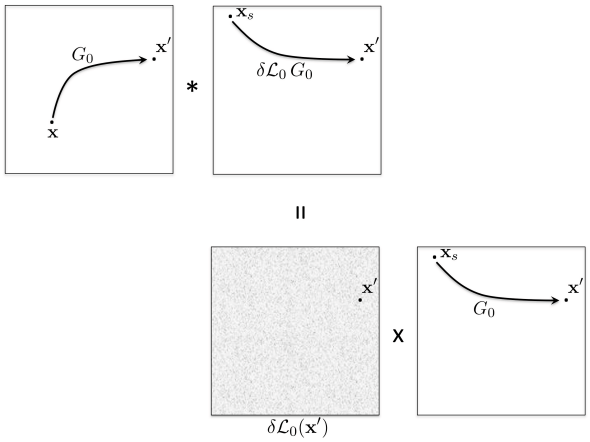

Figure 9: Term 8, Change in G_S due to single-scattering of the reference field by the reference secondary potencial.

In this new parametrization, the weighted changes in the model must be written as

$$\begin{bmatrix} \boldsymbol{\delta K_0^k} \\ \boldsymbol{\delta \rho_0^k} \\ \boldsymbol{\delta \Delta K^k} \\ \boldsymbol{\delta \Delta \rho^k} \end{bmatrix} = \begin{bmatrix} \boldsymbol{\delta K_{0,0}^k} \\ \boldsymbol{\delta \rho_{0,0}^k} \\ \mathbf{0} \\ \mathbf{0} \end{bmatrix} + \begin{bmatrix} \boldsymbol{\delta K_{0,S}^k} \\ \boldsymbol{\delta \rho_{0,S}^k} \\ \boldsymbol{\delta \Delta K^k}_{,S} \\ \boldsymbol{\delta \Delta \rho^k}_{,S} \end{bmatrix} = \begin{bmatrix} \boldsymbol{\delta K_{0,0}^k} \\ \boldsymbol{\delta \rho_{0,0}^k} \\ \mathbf{0} \\ \mathbf{0} \end{bmatrix} + \sum_{i=1}^{n=8} \begin{bmatrix} \boldsymbol{\delta K_{0,S}^{k,i}} \\ \boldsymbol{\delta \rho_{0,S}^{k,i}} \\ \boldsymbol{\delta \Delta K^{k,i}}_{,S} \\ \boldsymbol{\delta \Delta \rho^{k,i}}_{,S} \end{bmatrix}. \quad (25)$$

From (22) and (23) we can evaluate the weighted changes in the model for a given pair $(\boldsymbol{x}_g;\boldsymbol{x}_s)$ by

$$\begin{bmatrix} \boldsymbol{\delta K_{0,0}^k} \\ \boldsymbol{\delta \rho_{0,0}^k} \end{bmatrix} = \begin{bmatrix} \boldsymbol{U_0}^\dagger \\ \boldsymbol{V_0}^\dagger \end{bmatrix} \widehat{\delta G}_0, \quad (26)$$

and

$$\begin{bmatrix} \boldsymbol{\delta K_{0,S}^{k,i}} \\ \boldsymbol{\delta \rho_{0,S}^{k,i}} \\ \boldsymbol{\delta \Delta K^{k,i}}_{,S} \\ \boldsymbol{\delta \Delta \rho^{k,i}}_{,S} \end{bmatrix} = \begin{bmatrix} \boldsymbol{U}_i^\dagger \\ \boldsymbol{V}_i^\dagger \\ \boldsymbol{U}_{\boldsymbol{\Delta},i}^\dagger \\ \boldsymbol{V}_{\boldsymbol{\Delta},i}^\dagger \end{bmatrix} \widehat{\delta G}_S. \quad (27)$$

Evaluation of $\boldsymbol{\delta K_0^k}$

As seen in (25), each weighted change in the model is composed of 9 terms. But, due to similarities in the format of theses terms, we need only to evaluate 2 of them. The others come from those two easily. Let's see those two terms for $\boldsymbol{\delta K_0^k}$.

The first term evaluated is $\boldsymbol{\delta K_{0,0}^k}$. If we consider $\boldsymbol{\delta \rho_0} = \mathbf{0}$, (17) becomes, in the frequency domain,

$$\widehat{\delta G}_0(\boldsymbol{x}_g;\boldsymbol{x}_s) = -\int_{\mathbb{V}} d^3\boldsymbol{x}' \, \frac{\omega^2}{K_0^2(\boldsymbol{x}')} \widehat{G}_0(\boldsymbol{x}';\boldsymbol{x}_g) \widehat{G}_0(\boldsymbol{x}';\boldsymbol{x}_s) \, \delta K_0(\boldsymbol{x}'). \quad (28)$$

Using (26), we get

$$\delta K_{0,0}^k(\boldsymbol{x}_i') = -\frac{\omega^2}{K_0^2(\boldsymbol{x}_i')} \overbrace{\widehat{G}_0^*(\boldsymbol{x}_i';\boldsymbol{x}_s)}^{\text{direct wavefield cross-corralation}} \underbrace{\widehat{G}_0^*(\boldsymbol{x}_i';\boldsymbol{x}_g) \widehat{\delta G}_0(\boldsymbol{x}_g;\boldsymbol{x}_s)}_{\text{back-propagation of } \widehat{\delta G}_0}. \quad (29)$$

Figure 10 shows a cartoon that represents the operation above.

Comparing (28) with the third to the eighth term of (21), keeping $\boldsymbol{\delta \rho_0} = \mathbf{0}$, we see that $\boldsymbol{\delta K_{0,S}^{k,3}}$ to $\boldsymbol{\delta K_{0,S}^{k,8}}$ are similar to $\boldsymbol{\delta K_{0,0}^k}$ provided the suitable substitutions of the G_0's by the G_S's, and $\widehat{\delta G}_0$ by $\widehat{\delta G}_S$.

The second term evaluated is $\boldsymbol{\delta K_{0,S}^{k,1}}$. Analogously to the previous term, we consider $\boldsymbol{\delta \rho_0} = \mathbf{0}$. So, in the frequency domain, the first term of (21) becomes

$$\delta K_{0,0}^k(\mathbf{x}_i') = -\frac{\omega^2}{K_0^2(\mathbf{x}_i')} \overbrace{\widehat{G}_0^*(\mathbf{x}_i';\mathbf{x}_s)}^{\text{crosscorrelation}} \underbrace{\widehat{G}_0^*(\mathbf{x}_i';\mathbf{x}_g) \delta \widehat{G}_0(\mathbf{x}_g;\mathbf{x}_s)}_{\text{back-propagation of } \delta \widehat{G}_0}$$

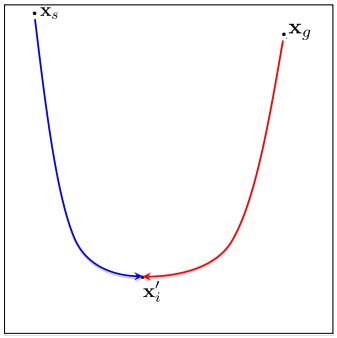

Figure 10: Evaluating the weighted change in the reference part of the bulk modulus due to the reference wavefield residual $\widehat{\delta G}_0$. In red, we see the back-propagation of the reference wavefield residual $\widehat{\delta G}_0$ from the receiver; in blue, we see the direct reference wavefield from source; a cross-correlation of both wavefields are performed at point $\boldsymbol{x}_i'$.

domain, the first term of (21) becomes

$$\widehat{\delta G}_{S,1}(\boldsymbol{x}_g;\boldsymbol{x}_s) = \int_{\mathbb{V}} d^3\boldsymbol{x}' \, \widehat{G}_0(\boldsymbol{x}';\boldsymbol{x}_g) \mathcal{V}(\boldsymbol{x}') \left[\int_{\mathbb{V}} d^3\boldsymbol{x}'' \, \frac{\omega^2}{K_0^2(\boldsymbol{x}'')} \widehat{G}_0(\boldsymbol{x}'';\boldsymbol{x}') \widehat{G}_0(\boldsymbol{x}'';\boldsymbol{x}_s) \, \delta K_0(\boldsymbol{x}'') \right]. \quad (30)$$

Using (27), we get

$$\delta K_{0,S}^{k,1}(\boldsymbol{x}_i'') = \int_{\mathbb{V}} d^3\boldsymbol{x}' \, \frac{\omega^2}{K_0^2(\boldsymbol{x}_i'')} \underbrace{\widehat{G}_0^*(\boldsymbol{x}_i'';\boldsymbol{x}_s)}_{\text{direct wavefield cross-correlation}} \underbrace{\widehat{G}_0^*(\boldsymbol{x}_i'';\boldsymbol{x}')}_{\text{Second back-propagation}} \underbrace{\mathcal{V}(\boldsymbol{x}')}_{\text{weighting by the reflectors/scatterers}} \underbrace{\widehat{G}_0^*(\boldsymbol{x}';\boldsymbol{x}_g) \widehat{\delta G}_S(\boldsymbol{x}_g;\boldsymbol{x}_s)}_{\text{back-propagation}}. \quad (31)$$

sum over all possible reflector/scatterer locations

Summary and Conclusions

In this paper we present a decomposition of current full-waveform inversion (FWI) sensitivity kernels into several sub-kernels using a scattering formulation that relies on decomposing the model space into smooth and singular model components. It is important to note that while the superposition of all our sub-kernels yields a Frèchet gradient that is no different than those currently use in FWI, each individual sub-kernel has different contributions in terms of nonlinearity with respect to both model and data components. We show that the contributions of each sub-kernel can be in fact physically interpreted in terms of orders of scattering with respect to the unknown model

$$\delta K^{k,1}_{0,S}(\mathbf{x}''_i) = \int_{\mathbb{V}} d^3\mathbf{x}' \frac{\omega^2}{K^2_0(\mathbf{x}''_i)} \widehat{G}^*_0(\mathbf{x}''_i;\mathbf{x}_s)\widehat{G}^*_0(\mathbf{x}''_i;\mathbf{x}')\mathcal{V}(\mathbf{x}')\widehat{G}^*_0(\mathbf{x}';\mathbf{x}_g)\delta\widehat{G}_S(\mathbf{x}_g;\mathbf{x}_s)$$

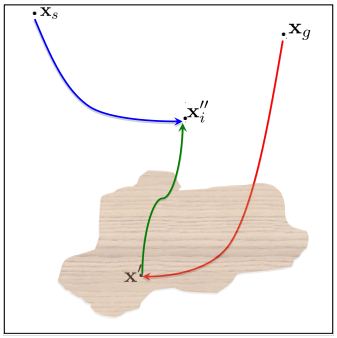

Figure 11: Evaluating the first-term contribution for weighted change in the reference part of the bulk modulus due to the scattered wavefield residual $\widehat{\delta G_S}$. In red, we see the back-propagation of the reference wavefield residual $\widehat{\delta G_S}$ from the receiver; in yellow, the weighting by the scattering potencial; in green, the second back-propagation from the weighting point to $\boldsymbol{x}'_i$; in blue, we see the direct reference wavefield from source; a cross-correlation of both wavefields are performed at point $\boldsymbol{x}''_i$.

parameters. Thus, using our scattering parameterization and sub-kernel approach in FWI practice will in principle allow for better control of nonlinear effects at each iteration of FWI model optimization.

In addition to its potential benefits in controlling convergence of FWI routines, we point out that the underlying scattering formulation of our method allows for a direct connection to migration-type imaging and model building. Migrated seismic images can in principle be taken an estimate for the sharp/singular part of the subsurface model, while models from velocity analysis are a proxy for the smooth model component. Under that framework, our formalism provides for an explicit method for jointly using velocity models and migrated seismic images in FWI as well as for understanding their interplay in the model-building process. Likewise, the scattering kernels presented here can be directly used in the the context of extended images (EIs) in devising nonlinear wave-equation migration velocity model building techniques. In practice, we expect challenges to arise when choosing how to separate/represent the smooth and sharp model components, and when decomposing the corresponding data components. So while there are potential benefits in describing and including higher-order nonlinear terms in FWI using our formulation, achieving them in practice with both synthetic and field data is the subject of ongoing research.

References

Lailly, P., 1983, The seismic inverse problem as a sequence of before stack migrations: Inverse scattering theory and application, Society for Industrial and Applied Mathematics (SIAM), 206–220.

Rickett, J. E., and P. C. Sava, 2002, Offset and angle-domain common image-point gathers for shot-profile migration: Geophysics, **67**, 883–889.

Sava, P., and I. Vasconcelos, 2009, Extended common-image-point gathers for wave-equation migration: EAGE Exp. Abs.

———, 2010, Extended imaging conditions for wave-equation migration. Geophys. Prosp, accepted.

Sava, P. C., and S. Fomel, 2003, Angle-domain common-image gathers by wavefield continuation methods: Geophysics, **68**, 1065–1074.

Symes, W. W., 2008, Migration velocity analysis and waveform inversion: Geophysical Prospecting, **56**, 765–790.

Tarantola, A., 1984, Inversion of seismic reflection data in the acoustic approximation: Geophysics, **49**, 1259–1266.

———, 1986, A strategy for nonlinear elastic inversion of seismic reflection data: Geophysics, **51**, 1893–1903.

Vasconcelos, I., 2008, Generalized representations of perturbed fields – applications in seismic interferometry and migration: SEG Exp. Abs.

Vasconcelos, I., P. Sava, and H. Douma, 2009, Wave-equation extended images via image-domain interferometry: EAGE Exp. Abs.

———, 2010, Nonlinear extended images via image-domain interferometry: Geophysics, **75**, SA105–SA115.

Vigh, D., E. W. Starr, and J. Kapoor, 2009, Developing earth models with full waveform inversion: The Leading Edge, **28**, 432–435.

Virieux, J., and S. Operto, 2009, An overview of full-waveform inversion in exploration geophysics: Geophysics, **74**, WCC1–WCC26.

Acknowledgments

I'd like to thank Jörg Schleicher for the support and help in revising and discussing the ideas shown here; and the CEPETRO-UNICAMP[5] for the scholarship.

[5]Centro de estudo do petróleo - Universidade Estadual de Campinas